Featured in Physics

Detecting partial synchrony in a complex oscillatory network using pseudovortices

Yasuhiro Yamada [*,†] and Kensuke Inaba [*]

NTT Basic Research Laboratories, NTT Corporation, 3-1 Morinosato Wakamiya, Atsugi, Kanagawa 243-0198, Japan

(Received 16 February 2023; accepted 23 June 2023; published 17 August 2023)

Partial synchronization is an important dynamical process of coupled oscillators on various natural and artificial networks, which can remain undetected due to the system complexity. With an analogy between pairwise asynchrony of oscillators and topological defects, i.e., vortices, in the two-dimensional XY model, we propose a robust and data-driven method to identify the partial synchronization on complex networks. The proposed method is based on an integer matrix whose element is pseudovorticity that discretely quantifies asynchronous phase dynamics in every two oscillators, which results in graphical and entropic representations of partial synchrony. As a first trial, we apply our method to 200 FitzHugh-Nagumo neurons on a complex small-world network. Partially synchronized chimera states are revealed by discriminating synchronized states even with phase lags. Such phase lags also appear in partial synchronization in chimera states. Our topological, graphical, and entropic method is implemented solely with measurable phase dynamics data, which will lead to a straightforward application to general oscillatory networks including neural networks in the brain.

DOI: 10.1103/PhysRevE.108.024307

I. INTRODUCTION

Synchronization is a universal phenomenon in a system of interacting oscillators whose relative phases are fully locked in the whole system [1]. In recent decades, partial synchronization of oscillators has also been recognized as ubiquitous and important in broad research fields through extensive chimera studies originating from seminal theoretical papers [2,3]. At the beginning, chimera states denoted self-sustained heterogeneous states composed of synchronous and asynchronous oscillators with a symmetry breaking in homogeneous oscillators, e.g., a ring of identical phase oscillators [2,3]. Chimera states are found in experiments on optical [4–9], chemical [10–14], mechanical [15,16], and electronic [17–20] oscillators. Recently, the term is generally used for partially synchronized states appearing in various fields on physics, chemistry, biology, engineering, and social networks, irrespective of the presence of the symmetry breaking [21–26]. In fact, partially synchronized chimera-like phenomena possibly have significant influence on the functionalities and health of brain neurons [27–31], on heart rhythm [32], on power-grid networks [33], and on cluster synchronization on irregular graphs [20,34–41], which have inherent inhomogeneity on complex networks.

Our motivation is to quantify the expanding partial synchrony on complex networks in a robust and data-driven way. In the original chimera studies on a regular ring, two kinds of synchrony based on frequency and phase were used to clarify the chimera states [2,3]. Frequency synchronization indicates that synchronized oscillators possess the same oscillation frequency as a result of entrainment. A distribution of mean or instantaneous frequency is often used to detect the partial frequency synchrony, where the coexistence of synchronized oscillators with the same frequency and desynchronized ones with distributed frequency indicates a chimera state [2,3,9,11,13–15,18]. While the frequency synchrony qualitatively reveals the chimera states with a look at the distribution, phase synchrony has been utilized to quantify chimeras sufficiently. A region of oscillators is obviously synchronized with spatial coherence when the oscillators are almost in-phase at a time, which can be easily checked with the phase snapshot [2–5,7–9,11,12,14–19]. The spatial synchrony is quantified by the distribution of the local order parameter $r_x = |\sum_{x'} g(x,x')\exp(i\theta_{x'})|$ where $g(x,x')$ determines the local vicinity of an oscillator at a position x [2,3,10,11,13,14]. The order parameter is also utilized for analytical investigations of chimera states [2,3,42–45]. To quantify the in-phase synchrony more clearly, Kemeth *et al.* introduced the local curvature or the pairwise Euclidean distance of oscillator phases, and proposed chimera measures with a threshold for the spatial coherence to classify the chimera states [46], which has been successively used to detect experimental chimeras [7,9]. The frequency and in-phase synchronies are interchangeable in original chimera studies, where the partially frequency-synchronized oscillators are almost in-phase [2,3]. For other chimera measures based on frequency and phase synchrony, see review [26].

However, we sometimes face difficulties in quantifying the partial synchrony apart from the original context. For instance, quantitative indices of the spatial phase coherence can miss the synchrony that occurs remotely on an irregular graph [35] or that occurs with twisted (spiral) waves [14,32,47–49]. Although the remotely synchronized clusters can be predicted by local symmetries of the graph [36], we need to know the precise network structure and the exact equation of motion for oscillators, which are not necessarily accessible in actual

[*]These authors contributed equally to this work.
[†]yshr.yamada@ntt.com

 ©2023 American Physical Society

experiments. With the expanding interest in partial synchrony, we will obtain more dynamics data in noisy experiments of oscillators on complex networks with unknown details, in which synchrony can be hidden behind the complex dynamics. To analyze the noisy data by algorithms and utilize the synchronization for applications, like for optimization in an optoelectric experiment [50], developing a robust and quantitative concept of synchrony based on measurable variables is desirable in this data-driven era.

In this paper, we propose a discrete analog of frequency synchrony with an analogy between partial asynchrony and topological defects, *vortices*, in the two-dimensional XY model [51–53] to quantify the expanding partial synchrony clearly and robustly: no vortex in a space-time ($1+1$-dimensional) plane means synchrony. Using the analogy, we discretely quantify the accumulated phase mismatch between every two oscillators during a period, which leads to an integer matrix I. We note that the matrix can be calculated solely from oscillator phase dynamics data without knowledge of the network structure or theoretical model that describes the oscillator dynamics. The element I_{ij} is *pseudovorticity* that counts pairwise asynchrony between ith and jth oscillators. To quantify the partial synchronization in a whole system, we next introduce a graph from the matrix, named a *synchronization graph*, where synchronous oscillators are connected with each other irrespective of the original network structure. From the synchronization graph, we identify the clique clusters in which all oscillators are mutually synchronized by solving a clique problem of the graph. The size distribution of the clusters gives an entropic measure that quantifies the disorder of the synchronization, which becomes a useful measure of chimera states. The partially synchronized states are further classified by *frequency divergence* obtained from the pseudovorticity matrix. Numerical simulations confirm that these measures identify different phases in the parameter space of FitzHugh-Nagumo (FHN) neurons [54,55] on a small-world network [56] with high clustering and a short path length. The FHN neuron is a brain-inspired neuronal oscillator, which has been used extensively in research on chimera states on a one-dimensional ring [19,57,58], empirical brain networks [59–61], and networks with complex topology [62–64]. Network small-worldness is one of the important features of actual neural networks [56]. We emphasize that our method property identifies synchronization with a gradating phase lag and the related chimeras without additional human confirmation, which cannot be identified by previous chimera measures.

II. THEORETICAL FRAMEWORK

A topological index can be useful for a robust classification of a system in general because it gives a measure of fundamental classification without information on the fine details of the system. A famous example is the topological defects in the two-dimensional XY spin model, which characterize the low energy excitations in the system and account for the topological phase transition [51–53]. The XY spin at two-dimensional position $\vec{r}=(x,y)$ is characterized by an angle $\theta(\vec{r})$. A topological defect is discretely quantified by the integer vorticity

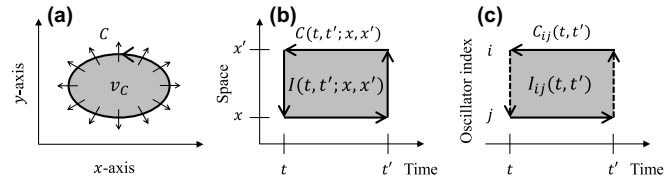

FIG. 1. Schematic illustrations of closed paths for calculating vorticity and pseudovorticity. (a) Vorticity v_C bounded by a closed curve C in two-dimensional phase field $\theta(x,y)$. (b) Vorticity $I(t,t';x,x')$ bounded by a closed rectangular $C(t,t';x,x')$ in $1+1$-dimensional phase field $\theta(t,x)$. (c) Pseudovorticity $I_{ij}(t,t')$ defined in between oscillator i and j.

obtained from an integral of the spin angle along a closed path as shown in Fig. 1(a); $v_c=\frac{1}{2\pi}\oint_C \vec{\nabla}\theta(\vec{r})\cdot d\vec{r}=\frac{1}{2\pi}\oint_C d\theta$.

Similarly, we introduce an integer index that characterizes the partial synchronization. As a preparation for the following discussion, we consider a one-dimensional oscillator field $\theta(t,x)$ whose phase continuously changes along the continuous x axis as well as along time. In this case we can define a topological quantity by an integral of the phase field as a function of time and position on a closed path $C(t,t';x,x')$ as in Fig. 1(b):

$$I(t,t';x,x') := \frac{1}{2\pi}\oint_{C(t,t';x,x')} d\theta(t,x), \tag{1}$$

which represents an integer vortex strength generated by the phase field on the $1+1$-dimension. The zero value $I(t,t';x,x')=0$ is necessary for the condition that the domain from x to x' is synchronized during the time evolution from t to t' with no accumulated vortex. Then, we can relate the partial synchronization with the integral.

The integral of the phase field is, however, not well defined in the case of the discrete oscillators considered here because the phase may discontinuously change along the oscillator index with a phase ambiguity of the amount of 2π. We here define an analogous index by dividing the closed path into the continuous changing parts along the time and discontinuous changing parts along the oscillator index as shown in Fig. 1(c):

$$I_{ij}(t,t') := \frac{1}{2\pi}\Bigg[\int_{\theta_j(t)}^{\theta_j(t')} d\theta_j(t) + \int_{\theta_i(t')}^{\theta_i(t)} d\theta_i(t) + \mathrm{Arg}(e^{i[\theta_i(t')-\theta_j(t')]}) + \mathrm{Arg}(e^{i[\theta_j(t)-\theta_i(t)]})\Bigg], \tag{2}$$

where the argument function $\mathrm{Arg}(z)$ terms account for the phase difference between ith and jth oscillators at the initial and the final times t and t'. It is noteworthy that the index is an integer, $I_{ij}(t,t')=\lfloor\frac{1}{2}+\frac{\theta_j(t')-\theta_i(t')}{2\pi}\rfloor+\lfloor\frac{1}{2}+\frac{\theta_i(t)-\theta_j(t)}{2\pi}\rfloor$, that is associated with the pseudovortex strength inside the shaded box in Fig. 1(c). The pseudovorticity is directly related to the phase difference between two oscillators accumulated during the time interval, $\Delta\Phi_{ij}(t,t') := \theta_j(t')-\theta_j(t)-\theta_i(t')+\theta_i(t)$, by the following inequality:

$$\left\lfloor\frac{\Delta\Phi_{ij}(t,t')}{2\pi}\right\rfloor \leqslant I_{ij}(t,t') \leqslant \left\lfloor\frac{\Delta\Phi_{ij}(t,t')}{2\pi}\right\rfloor + 1. \tag{3}$$

To see the physical meaning clearly, we consider a simple case where all oscillators have definite harmonic motions,

$\theta_i(t) = 2\pi f_i t + \phi_i$. In this case, the pseudovorticity holds the inequality $\lfloor (f_j - f_i)(t' - t) \rfloor \leqslant I_{ij}(t, t') \leqslant \lfloor (f_j - f_i)(t' - t) \rfloor + 1$, which clearly indicates that the integer element approximately gives the phase difference accumulated by the time-evolution, $I_{ij}(t, t') \sim (f_j - f_i)(t' - t)$.

For n oscillators, we have an integer $n \times n$ matrix I whose elements are given by the pseudovorticities. The *pseudovorticity matrix* satisfies a couple of symmetries. The matrix is almost antisymmetric in terms of the oscillator index and time variables: $I(t, t') = -I^T(t, t')$ and $I(t, t') = -I(t', t)$. It holds the following triangle identity in time almost everywhere: $I(t_1, t_2) + I(t_2, t_3) + I(t_3, t_1) = O$. These symmetries are broken only for the negligible cases where the phase difference between two oscillators at the initial or final measurement time is the same as π modulo 2π (for details see Appendix A). A similar identity for the node indices does not hold in general due to the discontinuous phase change along the oscillator index: $I_{ij}(t, t') + I_{jk}(t, t') + I_{ki}(t, t') \neq 0$.

It is noteworthy that the measurement time interval $\Delta t := |t' - t|$ is important to distinguish desynchronization from synchronization. Obviously, for $\Delta t \to 0$, the pseudovorticity matrix trivially becomes the $n \times n$ null matrix, which seemingly indicates the synchronization for any case since we need a finite interval Δt to discriminate the desynchronization of two oscillators from the frequency synchronization. The minimum requirement of the time interval is approximately given by the minimum frequency difference $\Delta f_{\min}$ among all oscillators, $\Delta t \approx |\Delta f_{\min}|^{-1}$. However, the minimum value is usually unclear before executing a measurement or a numerical simulation in actual cases, which means that a given measurement interval Δt determines a resolution of frequency synchrony. Then, we need to carefully check whether a given Δt is enough to distinguish synchronization from desynchronization or not by changing its value. Furthermore, Δt is also related to the fundamental trade-off between resolutions of timing (time) and frequency to detect a transient synchronization; a longer measurement interval Δt provides a finer resolution in frequency, while it also gives rise to a reduction in detectability to the time-dependence of synchronization.

The pseudovorticity matrix includes the information on pairwise synchrony of every two oscillators. To quantify the partial synchronization in a whole system, we introduce a graphical representation of the (partially) synchronized groups of oscillators with an adjacency matrix, A, whose elements are defined by

$$A_{ij}(t, t') = \begin{cases} 1 & |I_{ij}(t, t')| \leqslant c_s, \quad i \neq j, \\ 0 & \text{otherwise}, \end{cases} \tag{4}$$

where c_s is the synchrony criteria of pseudovorticity. From Eq. (3), $c_s = 0$ and $c_s = 1$ are sufficient and necessary conditions for $-2\pi \leqslant \Delta\Phi_{ij}(t, t') < 2\pi$, respectively. Hereafter, we take $c_s = 1$ to find the synchrony with the phase difference within 2π. The adjacency matrix $A(t, t')$ is symmetric because the pseudovorticity matrix $I(t, t')$ is antisymmetric.

Every two connected nodes in the *synchronization graph* with the adjacency matrix are pairwise synchronized. If there is a group of nodes connected completely, i.e., a clique, then every two nodes in the group are synchronized, and the group or clique represents a partial synchronization in all the oscillators. Here we divide all the nodes into synchronized clique groups. At the first step, we find the largest clique in the synchronization graph, which is the maximum clique problem of the graph and a basic NP hard problem in computer science. Computing all cliques requires an exponential time with increasing graph size in general, but can be available for a relatively small size or sparse graph. In addition, we can obtain the approximated solution by solving the corresponding optimization problem. With a numerical algorithm, we (approximately) obtain the largest clique of the graph. Next, we find the next largest clique in the graph after removing the maximum clique. By repeating the procedure iteratively, we can identify all the cliques which need to cover the graph and their sizes, $s_1, \ldots, s_m$, with m being the number of cliques. This procedure mathematically gives a partition of the oscillator set, which naturally induces an equivalence relation of partial synchrony on the oscillators.

From the clique sizes, we define the probability where a node belongs to the jth largest clique by

$$p_j = s_j/n \quad \text{for} \quad j = 1, \ldots, m, \tag{5}$$

where n is the total number of nodes. If a single clique can cover the graph with $p_1 = 1$, then the whole system is synchronized, where any node must belong to the unique maximum clique. On the other hand, if every node belongs to different cliques, the system is totally desynchronized with the uniform distribution, $p_1 = p_2 = \ldots = p_n = 1/n$. Therefore, the partiality of synchrony (the uniformness of the probability) is quantified by the entropy as

$$S_{\text{sync}} := -\sum_{j=1}^{m} p_j \ln p_j. \tag{6}$$

At $S_{\text{sync}} = 0$, the system seems to be synchronized with almost no vortex between every two nodes, while the system is completely desynchronized when the entropy has the maximum value, $S_{\text{sync}} = \log n$. In between them, the system comprises a mixture of several synchronized parts and desynchronized parts. Then, we here refer the entropy to as *synchronization entropy*.

In addition to the entropic measures, we calculate a characteristic frequency by using the measurement time interval and the pseudovorticity matrix,

$$\Delta f := \frac{||I(t, t')||_F}{\sqrt{2} n \Delta t}, \tag{7}$$

where $||A||_F$ denotes the Frobenius norm of a matrix A. We here refer to the frequency as *frequency divergence* because it physically means the typical frequency difference among oscillators. For instance, the frequency divergence is asymptotically equivalent to the standard deviation of the frequencies, $\Delta f \approx \sqrt{\frac{1}{n}\sum_{i=1}^{n}(f_i - \bar{f})^2}$, for noninteracting harmonic oscillators and a long interval Δt, where f_i and $\bar{f}$ are the individual frequencies and the average frequency of oscillators. If the frequency divergence is less than the inverse of the measurement time interval, then oscillators almost seem to have a single frequency in the measurement interval on average. Otherwise, the system includes oscillators with a

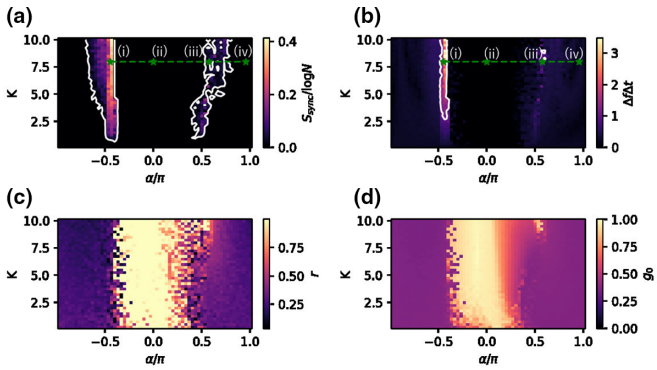

FIG. 2. False-color maps of synchronization measures of coupled FitzHugh-Nagumo neurons on a small-world network. (a) Synchronization entropy $S_{\rm sync}$, (b) Frequency divergence $\Delta f \Delta t$, (c) conventional phase order parameter r, and (d) relative size of the coherent component g_0. The horizontal and vertical axes represent the correlation lag α and the coupling strength K, respectively. The regions surrounded by white curves in panels (a) and (b) have $S_{\rm sync} > 0$ and $\Delta f \Delta t \geqslant 1$, respectively.

variety of frequencies:

$$\Delta f \Delta t \begin{cases} \ll 1 & \text{single-frequency oscillators,} \\ \gg 1 & \text{multifrequency oscillators.} \end{cases} \tag{8}$$

The condition on frequency divergence does not identify partial synchronizations because a partially synchronized oscillatory system may not have a difference in frequency on average. When most (but not all) of the oscillators are synchronized, the frequency divergence becomes very small as a chimera state as shown in Fig. 2(b). Nonetheless, it is helpful for classifying partial synchronizations further. For example, in Kuramoto and FHN oscillators on a ring structure, a desynchronized region in chimera states show frequency bands even though the original frequencies without interactions are unique [2,57,62]. The frequency divergence can capture such a change in the frequencies caused by interactions. Here, we explain the physical meaning of the frequency divergence. The frequency divergence is proportional to the Frobenius norm of the pseudovorticity matrix, $||I(t,t')||_F$, which physically corresponds to the variance of pseudovorticities. Since pseudovorticity is regarded as a discrete analog of the phase difference between two oscillators accumulated during the measurement time interval Δt, $||I(t,t')||_F/\Delta t$ is approximately proportional to the frequency variance. The factor $1/\sqrt{2}n$ in Δf is introduced for exact consistency with the frequency variance of harmonic oscillators with a sufficiently long measurement interval.

For a completely synchronized system, the proposed entropic and frequency measures must be zero. Therefore, they can be regarded as "disorder parameters," which are the order parameters of the desynchronization quantified from different points of view. These disorder parameters are complementary to the ordinal order parameter of complete phase synchronization, $r = |\sum_{j=1}^{n} \exp(i\theta_j)|/n$ [65]. The completely desynchronized state is characterized by the maximum entropy, $\log n$, while the frequency divergence has any finite value in this case. The maximum entropy state may hardly appear in the system with identical oscillators with a unique original frequency. Because the state requires a frequency difference larger than $\Delta f_{\rm min}$ for every two oscillators in spite of the fact that the oscillators have the same frequency in the noninteracting case. For systems with heterogeneous oscillators with a frequency band, which attract much attention in recent chimera studies, the completely desynchronized state can be found more easily. Our method is developed mainly for revealing hidden synchrony in the complex dynamics of the heterogeneous oscillators in a data-driven way.

The proposed method is simply based on basic concepts of topology, graph theory, and information theory, which are well developed in their fields. We can straightforwardly execute the method with a computational algorithm and raw phase dynamics data. Note that Boltzmann-Gibbs-Shannon entropy used in Eq. (6) is a choice to quantify the partiality of synchrony. Other possible choices are discussed in Appendix B.

III. APPLICATION TO FITZHUGH-NAGUMO NEURONAL OSCILLATORS ON A SMALL-WORLD NETWORK

As the first benchmark, we used the present synchronization measures to investigate the FHN model on a small-world network. The FHN model [54,55] is a simplification of the Hodgkin-Huxley model [66] that describes neuron dynamics. It has been pointed out that the small-worldness appears in a variety of systems, such as actual neuronal networks [56]. Thus, the following test case of the usage of our proposed method may extend to the empirical results obtained from actual brain experiments.

The dynamics of the FHN model is written as

$$\frac{1}{\tau}\frac{dv_i}{dt} = v_i - \frac{v_i^3}{3} - w_i + \cos\alpha \sum_j J_{ij} v_j + \sin\alpha \sum_j J_{ij} w_j, \tag{9}$$

$$\frac{dw_i}{dt} = a - bw_i + v_i + \cos\alpha \sum_j J_{ij} w_j - \sin\alpha \sum_j J_{ij} v_j, \tag{10}$$

where v and w are membrane potential and recovery variables, respectively, and α is a correlation lag. A coupling matrix J_{ij} is given by $J_{ij} = (K/N)a_{ij}$, where K is coupling strength, N is the number of sites, and a_{ij} is the adjacency matrix of a small-world graph. Other parameters are set as $a = 0.5$, $b = 0$, and $\tau = 0.05$. Small-world graph a_{ij} is created by the rewiring scheme proposed in Ref. [56] by starting from a_{ij} of a ring lattice of $N = 200$ sites with $k = 6$ edges. An obtained graph satisfies the characteristic of the small-world graph as follows. It has a clustering coefficient of 0.654, which is much greater than $k/n = 0.05$, and characteristic path length of 6.06, which is on the same order as $\ln(N)/\ln(k) = 2.30$, where k/n and $\ln(N)/\ln(k)$ are the clustering coefficient and characteristic path length of the corresponding random graph.

Figures 2(a) and 2(b) show the synchronization entropy $S_{\rm sync}$ and frequency divergence Δf as functions of correlation lag α and correlation strength K. The numerical simulation was done with the time difference $dt = 0.01$ and the number of time steps $N_{\rm step} = 40\,000$. We chose the time interval from $t = 360$ to $t' = 400$ when calculating $I_{ij}(t,t')$. Each phase of the neurons is defined by $\theta_j = \arg(v_j + iw_j)$. From these

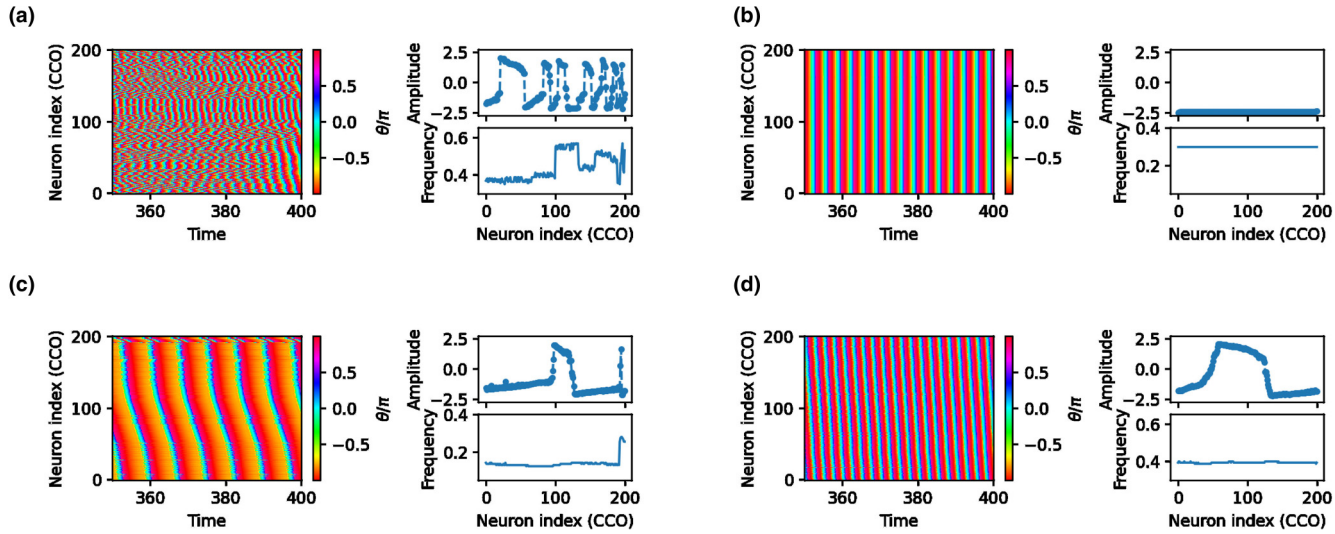

FIG. 3. Dynamics, snapshot, and mean frequency of reordered oscillators for several choices of the correlation lags depicted by stars on the synchronization phase diagram in Fig. 2. The correlation lags are set to $\alpha = -1.4, 0, 1.8$, and 3 for panels (a), (b), (c), and (d), respectively, with $K = 8$, which corresponds to the stars with indices (i)–(iv) in Figs. 2(a) and 2(b). In each parameter setting, the left panel shows the phase dynamics of coupled FitzHugh-Nagumo neurons reordered by their synchronization groups calculated for an interval from $t = 360$ to $t' = 400$ and their phases at $t = 400$. The right top panel is the snapshot of v-amplitudes at $t = 400$. The right bottom panel is the mean spiking frequencies of reordered neurons during the same interval. The dynamical states represent a chimera state, the complete synchronized state, a chimera state, and a synchronized state with gradational phase lag in panels (a), (b), (c), and (d), respectively.

measures, we can systematically determine the phase diagram even in a small-world graph that is a non-Euclid complex system. From these results, we found that synchronized region with $S_{\rm sync} = 0$ and $\Delta f = 0$ widely spreads at around $\alpha = 0$ and $(\pm)\pi$. Two main islands of chimera states with $0 < S_{\rm sync}/\log n \ll 1$ and $\Delta f > 0$ are revealed in the synchronized sea at around $\alpha = \pm\pi/2$, which are shown as regions surrounded by white curves in Fig. 2(a). On the one hand, the frequency is divergent at the middle in the left island at around $\alpha = -\pi/2$. On the other hand, the frequency almost stays $\Delta f \Delta t \lesssim 1$ in the right island chain. The difference between the left and right chimera regions are further discussed later with reference to Fig. 3.

Figure 2(c) shows a total order parameter defined as $r = |\sum_j \exp(i\theta_j)|/N$, which characterizes the complete synchronization. We can confirm that the synchronization sea at around $\alpha = 0$ corresponds to the conventional synchronous phase. By comparing r with our proposed measures, we also found another type of synchronized phase at around $\alpha = \pm\pi$, where the total order parameter r does not develop. As discussed below, this phase is a synchronized state with a gradational phase lag. In the chimera regions, r is small as expected.

Figure 2(d) shows temporal average of $g_0(t)$, where $g_0(t) = \int_0^\delta g(|D_{ij}|, t) d|D_{ij}|$, $D_{ij} = \exp(i\theta_i) - \exp(i\theta_j)$, and $g(|D_{ij}|, t)$ is a density function of $|D_{ij}|$ with a threshold for spatial coherence $\delta = 0.01 D_{\max}$ [46]. This $g_0(t)$ corresponds to the relative size of the coherent component, and thus $g_0(t) = 1$ means the complete synchronization. We found that this quantity successfully captures the synchronization phase, while, unfortunately, it cannot distinguish the other phases. Almost all regions except for the synchronized region at around $\alpha \sim 0$ seem to be chimera states. The specific synchronized state with a gradational phase lag is overlooked by $g_0(t)$ as well as by r.

Figures 3(a)–3(d) show the dynamics of a phase $\theta = \arctan(w/v)$ from time $t = 350$ to $t = 400$, amplitudes of v components at $t = 400$, and mean spiking frequencies ω of each neuron for different values of alpha with $K = 8$, where these parameter points are shown as (i)–(iv) in Fig. 2(a). Note that the neuron indices are reordered firstly by the number of clique cluster to which they belonged and secondly by the values of the phase θ at $t = 400$, which is referred to here as clique cluster ordering (CCO). The ordering enables us to find a clear difference in dynamics among revealed phases. First, as shown in Fig. 3(b), the synchronized region shows constant spiking frequency and amplitudes. Second, Fig. 3(d) shows a constant spiking frequency and a gradual change in the amplitudes. This is the gradational phase lag synchronization state. Note that, the total order parameter cannot develop because of the gradational phase lag. Furthermore, due to this phase lag, a measure g_0 index misleads us so that we mistake the gradational synchronized state for chimera states. Third, in the chimera states shown in Figs. 3(a) and 3(c), some parts show that amplitudes of v and spiking frequencies largely fluctuate, corresponding to the desynchronized parts. The other parts show almost constant spiking frequencies with amplitudes like a gradational synchronized state. These results indicate the coexistence of desynchronized and synchronized parts. The feature of the desynchronized parts is consistent with the behavior of the FHN model on the ring lattice structure [57,62]. A phase gradation in the synchronized parts is a characteristic of this small-world network. Note that these chimera states have different characteristics: a dominant synchronous region in one [Fig. 3(c)] and multiple synchronous regions in the other [Fig. 3(a)], which cause the aforementioned

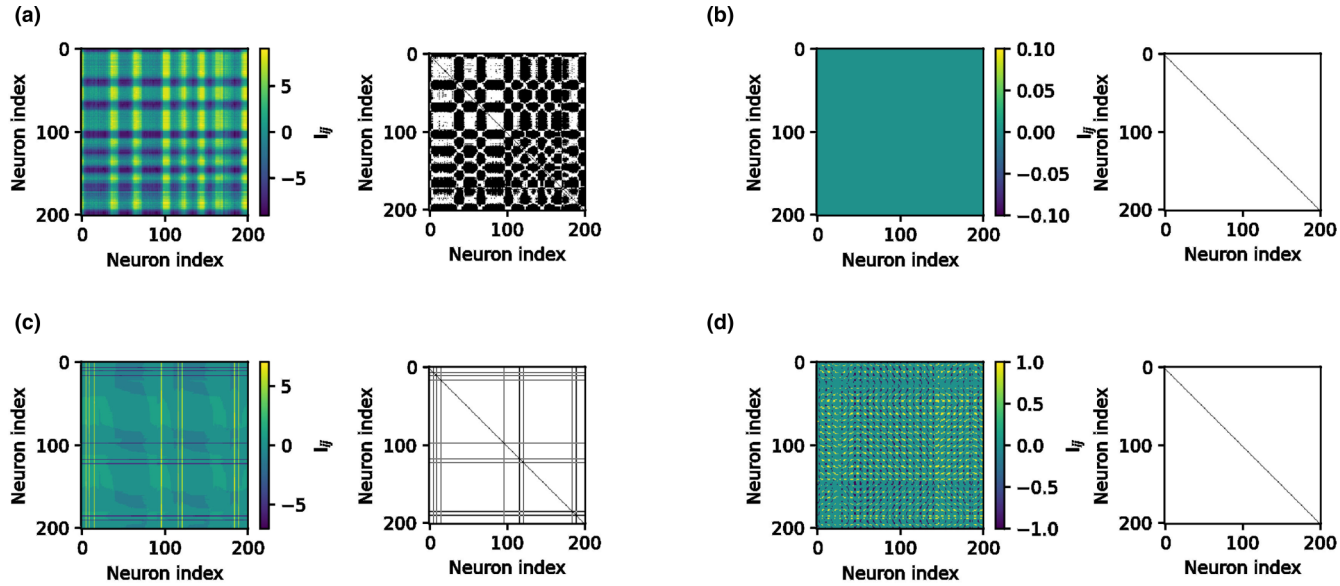

FIG. 4. False-color maps of pseudovorticity matrix and adjacent matrix of synchronization graph for coupled FitzHugh-Nagumo neuronal dynamics on a small-world network. We chose the correlation lags $\alpha = -1.4$, 0, 1.8, and 3 for panels (a), (b), (c), and (d), respectively, with $K = 8$, which corresponds to the parameter settings at stars with indices (i)–(iv) in Figs. 2(a) and 2(b). In each parameter setting, the left and right panels show the pseudovorticity matrix and adjacent matrix, respectively. These matrices correspond to a chimera state, the complete synchronized state, a chimera state, and a synchronized state with gradational phase lag in panels (a), (b), (c), and (d), respectively.

difference in $\Delta f \Delta t$. In this way, the present measures allow us to visualize the synchronous phase from the viewpoint of discrete frequency synchrony.

We next show in Figs. 4(a)–4(d) pseudovorticity matrix I_{ij} (left) and the adjacency matrix A_{ij} (right panel) of synchronization graph for four types of regions. We found that these four regions have distinct I_{ij} and A_{ij}. Figures 4(b) and 4(d) show that two types of synchronized regions have $|I_{ij}| \leqslant 1$ and complete graph of A_{ij}. Note that the gradational phase lag synchronization has $|I_{ij}| = 1$, while complete in-phase synchronization only has $|I_{ij}| = 0$. For the two types of the chimera regions in Figs. 4(a) and 4(c), the magnitudes of I_{ij} are large, and A_{ij} are sparse and rather dense, respectively. This is because the chimeras in Figs. 4(a) and 4(c) are close to the desynchronized and synchronized phases, respectively, which are consistent with the behavior in Figs. 3(a) and 3(c). These characteristics of I_{ij} provide a way to establish other good quantities in addition to S_{sync} to distinguish the different phases.

Figure 5(a) shows another entropic measure $S_{\max}$, which is defined in Appendix B. From this observation, we found

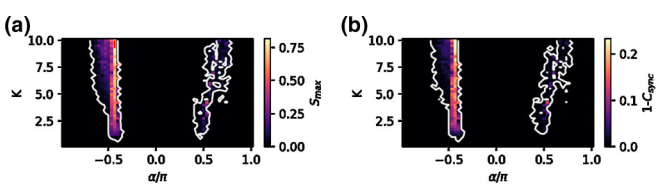

FIG. 5. (a) False-color maps of another entropic measure $S_{\max}$ and (b) clustering coefficient of synchronization graph C_{sync} for coupled FitzHugh-Nagumo neurons on a small-world network. The regions surrounded by white curves in panels (a) and (b) have $S_{\max} > 0$ and $1 > C_{\text{sync}}$, respectively.

that both S_{sync} and $S_{\max}$ provide qualitatively similar phase diagrams. $S_{\max}$ can be calculated with smaller numerical effort than S_{sync} can; namely, $S_{\max}$ is determined only from the largest clique without iterative clique determinations. These results suggest that the entropic definitions based on Schur-concave-function family will provide the similar results. Note that an iterative determination is required for visualizing all of the synchronized clusters of oscillators. Figure 5(b) shows the clustering coefficient C_{sync} of the synchronization graph, and $1 - C_{\text{sync}}$ has a structure remarkably similar to the entropic measures S_{sync} and $S_{\max}$. In particular, $S_{\max}$ and $1 - C_{\text{sync}}$ show good agreement with each other. The clustering coefficient may be useful for screening partial synchronizations in a large oscillatory system because it merely requires $O(n^3)$ calculation, which is much smaller than the cost to exactly solve the NP problem to obtain S_{sync}. We need further confirmation of the similarity between $1 - C_{\text{sync}}$ and S_{sync} in different systems. We note that the temporal change in the graph structure includes the information on the synchronization dynamics. A comparison between the synchronization graph and the original network graph would also be interesting, which will be discussed elsewhere.

To clarify the stability and scalability of the observed chimera states, we next systematically investigated the size N dependence of the phase diagram. Figure 6 shows the size dependence of S_{sync} and phase diagrams. Simply put, we found that qualitatively similar phase diagrams were observed as N increases with a fixed $k/N(=0.05)$, the ratio of the (averaged) number of edges and nodes. We also set the cluster coefficient C to similar values ranging within [0.5,0.6]. Due to the randomness of the created small world graphs [56], fluctuation of the cluster coefficient values remains. Irrespective of the small fluctuation of C and size N, we observed similar phase diagrams. This consistency of the phase diagrams suggests the

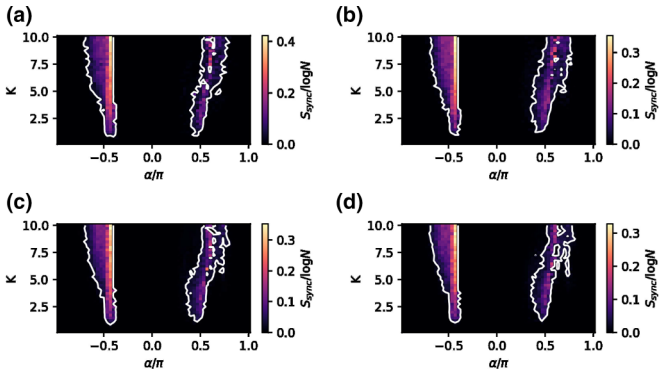

FIG. 6. Size dependence of the phase diagrams (false-color maps of S_{sync}) of FitzHugh-Nagumo neurons on small-world networks. The system sizes are set to $N = 200$, $N = 300$, $N = 400$, and $N = 500$ for (a), (b), (c), and (d), respectively. The regions surrounded by white curves have $S_{\text{sync}} > 0$. Here, the number of edges k is scaled as $k = 0.05N$; namely, the ratio k/N is fixed. For different N, clustering coefficients are set to similar values ranging within $C \in [0.5, 0.6]$.

stability of the chimera states and supports the validity of our methods.

We further investigated the cluster coefficient C dependence of the phase diagram with a fixed $N = 200$. Figure 7 shows C dependence of S_{sync}. We found that, interestingly, the chimera phases become wider and wider as C becomes smaller and smaller. In particular, the chimera phase at around $\alpha = \pi/2$ significantly expands as C decreases. This can be attributed to the fact that when a small-world graph has a small C, which means that the graph is close to a random graph where the synchronized state becomes unstable, the chimera phase becomes stable instead of the synchronized phase. We found that the chimera states at around $\alpha = -\pi/2$ are robust to the change in C, while those at around $\alpha = \pi/2$ are sensitive to it. This may be attributed to the fact that the chimera states at around $\alpha = \pi/2$ consist of dominant phase-lagged synchronized oscillators and minority desynchronized ones

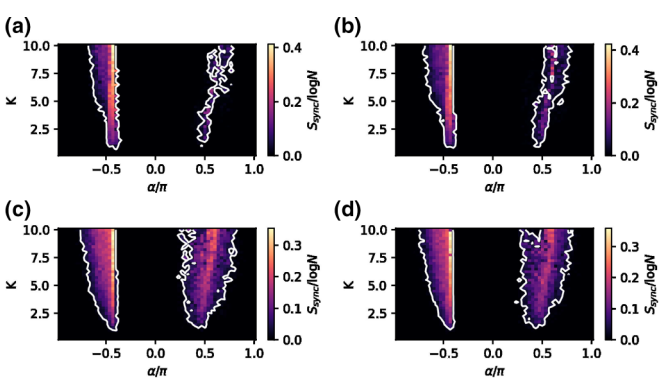

FIG. 7. Change in the phase diagrams (false-color maps of S_{sync}) of FitzHugh-Nagumo neurons on small-world networks having different clustering coefficients C and mean-path lengths L with a fixed $N = 200$. The coefficients and lengths are given by ($C = 0.65, L = 6.1$), ($C = 0.59, L = 3.8$), ($C = 0.50, L = 3.3$), and ($C = 0.33, L = 2.9$) for panels (a), (b), (c), and (d), respectively. The regions surrounded by white curves have $S_{\text{sync}} > 0$.

[see Fig. 3(c)], and thus the instability of the phase-lagged synchronization caused by the decrease in C significantly affects the phase diagrams.

IV. CONCLUSIONS

We have introduced a graphical description to classify complex synchronization dynamics in an oscillatory system based on a discrete analog of frequency synchrony. To make the partial synchronization visible in a computer-friendly way, we have proposed an index matrix with integer elements from a topological viewpoint. Each element of the matrix represents the pseudovorticity generated by the phase difference accumulated by the time-evolution of a pair of oscillators in the system. From the matrix, we derive a synchronization graph that represents the pairwise synchronization in a graphical way. The synchronized clusters of oscillators are clarified by solving a clique cover problem of the graph. From the pseudovorticity matrix and the synchronization graph, we can also obtain the synchronization entropy and the frequency divergence of the system, which are scalar measures for partial synchronization. We apply our method to coupled neuronal oscillators on a small-world network based on the FitzHugh-Nagumo model. From the analysis, we confirmed that our proposed measures work well for classification of the phase dynamics with a phase diagram, where we found complete synchronization, gradational synchronization, and chimera states.

In particular, the gradational synchronization and the related chimera states, which are hidden in the case of the original ordering of the oscillator index, are revealed by the reordering of the index based on the solution of the clique problem of the synchronization graph. The gradational synchronization missed in previous studies is one of the typical states, which dominates a large portion of the parameter space. As well as revealing the frequency synchronized state with spatial incoherence, we find the chimera state where synchronized and desynchronized states coexist accompanying the gradational phase lags.

For quantifying the synchrony, our method inspired by an analogy with vortices, which play a key role in a topological phase transition, gives complementary information to the Kuramoto order parameter defined in analogy to order parameters charactering phase transitions accompanied by spontaneous symmetry breaking [65]. In contrast to the Kuramoto order parameter, the proposed method ignores the presence of phase lags in synchrony, which simplifies the characterization of synchrony with a robust entropic measure for the partiality.

We expect that our method will also work well to classify and quantify the partial synchronization of general discrete oscillatory systems appearing not only in numerical simulations but also in actual experiments, e.g., electroencephalography (EEG) brain waves. An increase in partial synchrony on EEG signals for Parkinson's disease patients was found by the analysis based on pairwise order parameters [31], which quantify in-phase synchrony. With the proposed method, we can give a visualization of the synchronized clusters and may find further partial synchrony with phase lags missed in the previous research. Another possible application is in functional analysis

of neuromorphic devices. Adaptive and temporal changes in partial synchronization can be utilized for solving combinatorial optimization problems in photonic spiking neurons [50]. Our method may contribute to revealing the mechanism in a visual and quantitative way.

ACKNOWLEDGMENTS

We thank Takahiro Inagaki for valuable discussion and Hiroyuki Tamura for his support during this research.

APPENDIX A: SYMMETRIES OF PSEUDOVORTICITY MATRIX

The pseudovorticity matrix, $I(t,t')$, is antisymmetric in terms of the oscillator index and time variable except for conditions that have zero measure in the phase space, $\boldsymbol{\theta}$. The negligible conditions originate from the argument function used in Eq. (2), $\mathrm{Arg}(e^{ix}) = x + 2\pi\lfloor 1/2 - x/2\pi \rfloor$ for $x \in \mathbb{R}$, that lies within the interval $(\pi, \pi]$ and is discontinuous at $x \equiv \pi \bmod 2\pi$.

To provide more details, we start from the following equation of the matrix element:

$$I_{ij}(t,t') = \left\lfloor \frac{1}{2} + \frac{\theta_i(t) - \theta_j(t)}{2\pi} \right\rfloor + \left\lfloor \frac{1}{2} + \frac{\theta_j(t') - \theta_i(t')}{2\pi} \right\rfloor. \tag{A1}$$

The matrix element is determined by the phase differences at the initial and final measurement time. Here, we represent the phase differences by the integer quotients and the real remainders of the division by 2π:

$$\theta_i(t) - \theta_j(t) = -\pi + 2\pi k + 2\pi r, \tag{A2}$$

$$\theta_i(t') - \theta_j(t') = -\pi + 2\pi k' + 2\pi r', \tag{A3}$$

where we take $k, k' \in \mathbb{Z}$ and $r, r' \in [0, 1)$. Using these representations, we obtain the following equations:

$$I_{ij}(t,t') = 1 + k - k' + \lfloor -r' \rfloor, \tag{A4}$$

$$I_{ji}(t,t') = 1 + k' - k + \lfloor -r \rfloor. \tag{A5}$$

For $r, r' \in (0, 1)$, the element is thus antisymmetric:

$$I_{ij}(t,t') = -I_{ji}(t,t'). \tag{A6}$$

For $r = 0$ or $r' = 0$, where the phase difference is exactly $\pi \bmod 2\pi$, the element has no such symmetry. Since these conditions give lines (measure zero set) in two-dimensional Euclidean space, $(\theta_i(t), \theta_j(t))$ or $(\theta_i(t'), \theta_j(t'))$, we say that the pseudovorticity matrix is almost antisymmetric, and the exceptional cases are negligible for the actual analysis based on the numerical/experimental data of phase dynamics.

Similar arguments can be applied to the antisymmetry and the triangle equality in terms of time. We represent phase differences at $t = t_1, t_2$, and t_3 in a similar way:

$$\theta_i(t_1) - \theta_j(t_1) = -\pi + 2\pi k_1 + 2\pi r_1, \tag{A7}$$

$$\theta_i(t_2) - \theta_j(t_2) = -\pi + 2\pi k_2 + 2\pi r_2, \tag{A8}$$

$$\theta_i(t_3) - \theta_j(t_3) = -\pi + 2\pi k_3 + 2\pi r_3, \tag{A9}$$

where we take $k_1, k_2, k_3 \in \mathbb{Z}$ and $r_1, r_2, r_3 \in [0, 1)$. The matrix elements are represented as

$$I_{ij}(t_1,t_2) = 1 + k_1 - k_2 + \lfloor -r_2 \rfloor, \tag{A10}$$

$$I_{ij}(t_2,t_3) = 1 + k_2 - k_3 + \lfloor -r_3 \rfloor, \tag{A11}$$

$$I_{ij}(t_3,t_1) = 1 + k_3 - k_1 + \lfloor -r_1 \rfloor. \tag{A12}$$

For $r_1, r_2, r_3 \in (0, 1)$, the triangle equality and the antisymmetry is satisfied in terms of time:

$$I_{ij}(t_1,t_2) + I_{ij}(t_2,t_3) + I_{ij}(t_3,t_1) = 0, \tag{A13}$$

$$I_{ij}(t_1,t_2) = -I_{ij}(t_2,t_1). \tag{A14}$$

In other measure zero cases, these relations do not hold.

APPENDIX B: GENERALIZATION OF SYNCHRONIZATION ENTROPY

While we use Boltzmann-Gibbs-Shannon (BGS) entropy in Eq. (6), we have other choices for quantifying the uniformness of the size distribution in a partition of graph by cliques. In fact, we can obtain many entropylike measures by using Schur-concave functions. A Schur-concave function gives a monotone of majorization, that is a binary relation of two stochastic states which determines whether one state can be mapped from the other state by a doubly stochastic linear map or not. BGS entropy is one of such Schur-concave functions. Here, we introduce another Schur-concave function as

$$S_{\max} := 1 - \max(\boldsymbol{p}) = 1 - \frac{s_1}{n}. \tag{B1}$$

$S_{\max}$ is an intuitive measure of partial synchronization because $1 - S_{\max}$ is the largest cluster size, which contributes to a decrease in computing cost to solve the iterative clique problem if we don't need to know all the synchronized clusters of oscillators. It has the maximum $S_{\max} = (n-1)/n$ for desynchronization. In synchronized cases, $S_{\max}$ has the minimum $S_{\max} = 0$, whose value is the same as the synchronization entropy. We confirmed that $S_{\max}$ show a qualitatively similar phase diagram as that of synchronization entropy S_{sync} shown in Fig. 2 [see Fig 5(a)].

[1] A. Pikovskij, M. Rosenblum, and J. Kurths, *Synchronization: A Universal Concept in Nonlinear Sciences*, Cambridge Nonlinear Science Series (Cambridge University Press, Cambridge, UK, 2007).

[2] Y. Kuramoto and D. Battogtokh, Coexistence of coherence and incoherence in nonlocally coupled phase oscillators, Nonlinear Phenom. Complex Syst. **5**, 380 (2002).

[3] D. M. Abrams and S. H. Strogatz, Chimera States for Coupled Oscillators, Phys. Rev. Lett. **93**, 174102 (2004).

[4] A. M. Hagerstrom, T. E. Murphy, R. Roy, P. Hövel, I. Omelchenko, and E. Schöll, Experimental observation of chimeras in coupled-map lattices, Nat. Phys. **8**, 658 (2012).

[5] L. Larger, B. Penkovsky, and Y. Maistrenko, Laser chimeras as a paradigm for multistable patterns in complex systems, Nat. Commun. **6**, 7752 (2015).

[6] J. D. Hart, K. Bansal, T. E. Murphy, and R. Roy, Experimental observation of chimera and cluster states in a minimal globally coupled network, Chaos **26**, 094801 (2016).

[7] J. Shena, J. Hizanidis, V. Kovanis, and G. P. Tsironis, Turbulent chimeras in large semiconductor laser arrays, Sci. Rep. **7**, 42116 (2017).

[8] D. Brunner, B. Penkovsky, R. Levchenko, E. Schoell, L. Larger, and Y. Maistrenko, Spatio-temporal complexity in dual delay nonlinear laser dynamics: Chimeras and dissipative solitons, Chaos **28**, 103106 (2018).

[9] T. Makinwa, K. Inaba, T. Inagaki, Y. Yamada, T. Leleu, T. Honjo, T. Ikuta, K. Enbutsu, T. Umeki, R. Kasahara, K. Aihara, and H. Takesue, Experimental observation of chimera states in spiking neural networks based on degenerate optical parametric oscillators, Commun. Phys. **6**, 121 (2023).

[10] M. R. Tinsley, S. Nkomo, and K. Showalter, Chimera and phase-cluster states in populations of coupled chemical oscillators, Nat. Phys. **8**, 662 (2012).

[11] S. Nkomo, M. R. Tinsley, and K. Showalter, Chimera States in Populations of Nonlocally Coupled Chemical Oscillators, Phys. Rev. Lett. **110**, 244102 (2013).

[12] L. Schmidt, K. Schönleber, K. Krischer, and V. García-Morales, Coexistence of synchrony and incoherence in oscillatory media under nonlinear global coupling, Chaos **24**, 013102 (2014).

[13] M. Wickramasinghe and I. Z. Kiss, Spatially organized dynamical states in chemical oscillator networks: Synchronization, dynamical differentiation, and chimera patterns, PLoS ONE **8**, e80586 (2013).

[14] J. F. Totz, J. Rode, M. R. Tinsley, K. Showalter, and H. Engel, Spiral wave chimera states in large populations of coupled chemical oscillators, Nat. Phys. **14**, 282 (2018).

[15] E. A. Martens, S. Thutupalli, A. Fourrière, and O. Hallatschek, Chimera states in mechanical oscillator networks, Proc. Natl. Acad. Sci. USA **110**, 10563 (2013).

[16] T. Kapitaniak, P. Kuzma, J. Wojewoda, K. Czolczynski, and Y. Maistrenko, Imperfect chimera states for coupled pendula, Sci. Rep. **4**, 6379 (2015).

[17] L. Larger, B. Penkovsky, and Y. Maistrenko, Virtual Chimera States for Delayed-Feedback Systems, Phys. Rev. Lett. **111**, 054103 (2013).

[18] D. P. Rosin, D. Rontani, N. D. Haynes, E. Schöll, and D. J. Gauthier, Transient scaling and resurgence of chimera states in networks of Boolean phase oscillators, Phys. Rev. E **90**, 030902(R) (2014).

[19] L. V. Gambuzza, A. Buscarino, S. Chessari, L. Fortuna, R. Meucci, and M. Frasca, Experimental investigation of chimera states with quiescent and synchronous domains in coupled electronic oscillators, Phys. Rev. E **90**, 032905 (2014).

[20] B. Cao, Y. Wang, L. Wang, Y. Yu, and X. Wang, Cluster synchronization in complex network of coupled chaotic circuits: An experimental study, Front. Phys. **13**, 130505 (2018).

[21] M. J. Panaggio and D. M. Abrams, Chimera states: coexistence of coherence and incoherence in networks of coupled oscillators, Nonlinearity **28**, R67 (2015).

[22] E. Schöll, Synchronization patterns and chimera states in complex networks: Interplay of topology and dynamics, Eur. Phys. J. Spec. Top. **225**, 891 (2016).

[23] S. Majhi, B. K. Bera, D. Ghosh, and M. Perc, Chimera states in neuronal networks: A review, Phys. Life Rev. **28**, 100 (2019).

[24] Z. Wang and Z. Liu, A brief review of chimera state in empirical brain networks, Front. Physiol. **11**, 724 (2020).

[25] A. Zakharova, *Chimera Patterns in Networks: Interplay between Dynamics, Structure, Noise, and Delay*, Understanding Complex Systems (Springer International Publishing, Cham, 2020).

[26] F. Parastesh, S. Jafari, H. Azarnoush, Z. Shahriari, Z. Wang, S. Boccaletti, and M. Perc, Chimeras, Phys. Rep. **898**, 1 (2021).

[27] L. Mukhametov, A. Supin, and I. Polyakova, Interhemispheric asymmetry of the electroencephalographic sleep patterns in dolphins, Brain Res. **134**, 581 (1977).

[28] A. Rothkegel and K. Lehnertz, Irregular macroscopic dynamics due to chimera states in small-world networks of pulse-coupled oscillators, New J. Phys. **16**, 055006 (2014).

[29] G. G. Mascetti, Unihemispheric sleep and asymmetrical sleep: Behavioral, neurophysiological, and functional perspectives, Nat. Sci. Sleep **8**, 221 (2016).

[30] N. C. Rattenborg, B. Voirin, S. M. Cruz, R. Tisdale, G. Dell'Omo, H.-P. Lipp, M. Wikelski, and A. L. Vyssotski, Evidence that birds sleep in mid-flight, Nat. Commun. **7**, 12468 (2016).

[31] E. E. Asher, M. Plotnik, M. Günther, S. Moshel, O. Levy, S. Havlin, J. W. Kantelhardt, and R. P. Bartsch, Connectivity of EEG synchronization networks increases for Parkinson's disease patients with freezing of gait, Commun. Biol. **4**, 1017 (2021).

[32] E. M. Cherry and F. H. Fenton, Visualization of spiral and scroll waves in simulated and experimental cardiac tissue, New J. Phys. **10**, 125016 (2008).

[33] A. E. Motter, S. A. Myers, M. Anghel, and T. Nishikawa, Spontaneous synchrony in power-grid networks, Nat. Phys. **9**, 191 (2013).

[34] K. Kaneko, Clustering, coding, switching, hierarchical ordering, and control in a network of chaotic elements, Physica D **41**, 137 (1990).

[35] A. Bergner, M. Frasca, G. Sciuto, A. Buscarino, E. J. Ngamga, L. Fortuna, and J. Kurths, Remote synchronization in star networks, Phys. Rev. E **85**, 026208 (2012).

[36] V. Nicosia, M. Valencia, M. Chavez, A. Díaz-Guilera, and V. Latora, Remote Synchronization Reveals Network Symmetries and Functional Modules, Phys. Rev. Lett. **110**, 174102 (2013).

[37] P. Ashwin and O. Burylko, Weak chimeras in minimal networks of coupled phase oscillators, Chaos **25**, 013106 (2015).

[38] F. Sorrentino, L. M. Pecora, A. M. Hagerstrom, T. E. Murphy, and R. Roy, Complete characterization of the stability of cluster synchronization in complex dynamical networks, Sci. Adv. **2**, e1501737 (2016).

[39] M. T. Schaub, N. O'Clery, Y. N. Billeh, J.-C. Delvenne, R. Lambiotte, and M. Barahona, Graph partitions and cluster

synchronization in networks of oscillators, Chaos **26**, 094821 (2016).

[40] C. Bick, Isotropy of angular frequencies and weak chimeras with broken symmetry, J. Nonlinear Sci. **27**, 605 (2017).

[41] A. B. Siddique, L. Pecora, J. D. Hart, and F. Sorrentino, Symmetry- and input-cluster synchronization in networks, Phys. Rev. E **97**, 042217 (2018).

[42] D. M. Abrams, R. Mirollo, S. H. Strogatz, and D. A. Wiley, Solvable Model for Chimera States of Coupled Oscillators, Phys. Rev. Lett. **101**, 084103 (2008).

[43] C. Allefeld and S. Bialonski, Detecting synchronization clusters in multivariate time series via coarse-graining of Markov chains, Phys. Rev. E **76**, 066207 (2007).

[44] S. Bialonski and K. Lehnertz, Identifying phase synchronization clusters in spatially extended dynamical systems, Phys. Rev. E **74**, 051909 (2006).

[45] T. Kotwal, X. Jiang, and D. M. Abrams, Connecting the Kuramoto Model and the Chimera State, Phys. Rev. Lett. **119**, 264101 (2017).

[46] F. P. Kemeth, S. W. Haugland, L. Schmidt, I. G. Kevrekidis, and K. Krischer, A classification scheme for chimera states, Chaos **26**, 094815 (2016).

[47] L. S. Tsimring, N. F. Rulkov, M. L. Larsen, and M. Gabbay, Repulsive Synchronization in an Array of Phase Oscillators, Phys. Rev. Lett. **95**, 014101 (2005).

[48] D. A. Wiley, S. H. Strogatz, and M. Girvan, The size of the sync basin, Chaos **16**, 015103 (2006).

[49] T. Girnyk, M. Hasler, and Y. Maistrenko, Multistability of twisted states in nonlocally coupled Kuramoto-type models, Chaos **22**, 013114 (2012).

[50] T. Inagaki, K. Inaba, T. Leleu, T. Honjo, T. Ikuta, K. Enbutsu, T. Umeki, R. Kasahara, K. Aihara, and H. Takesue, Collective and synchronous dynamics of photonic spiking neurons, Nat. Commun. **12**, 2325 (2021).

[51] V. L. Berezinskii, Destruction of long-range order in one-dimensional and two-dimensional systems possessing a continuous symmetry group. I. Classical systems., Sov. Phys. JETP **32**, 493 (1971).

[52] V. L. Berezinskii, Destruction of long-range order in one-dimensional and two-dimensional systems possessing a continuous symmetry group. II. Quantum systems., Sov. Phys. JETP **34**, 610 (1972).

[53] J. M. Kosterlitz and D. J. Thouless, Ordering, metastability and phase transitions in two-dimensional systems, J. Phys. C: Solid State Phys. **6**, 1181 (1973).

[54] R. FitzHugh, Mathematical models of threshold phenomena in the nerve membrane, Bull. Math. Biophys. **17**, 257 (1955).

[55] J. Nagumo, S. Arimoto, and S. Yoshizawa, An active pulse transmission line simulating nerve axon, Proc. IRE **50**, 2061 (1962).

[56] D. J. Watts and S. H. Strogatz, Collective dynamics of "small-world" networks, Nature (London) **393**, 440 (1998).

[57] I. Omelchenko, O. E. Omelchenko, P. Hovel, and E. Scholl, When Nonlocal Coupling Between Oscillators Becomes Stronger: Patched Synchrony or Multichimera States, Phys. Rev. Lett. **110**, 224101 (2013).

[58] N. Semenova, A. Zakharova, V. Anishchenko, and E. Scholl, Coherence-Resonance Chimeras in a Network of Excitable Elements, Phys. Rev. Lett. **117**, 014102 (2016).

[59] T. Chouzouris, I. Omelchenko, A. Zakharova, J. Hlinka, P. Jiruska, and E. Schöll, Chimera states in brain networks: Empirical neural vs modular fractal connectivity, Chaos **28**, 045112 (2018).

[60] L. Ramlow, J. Sawicki, A. Zakharova, J. Hlinka, J. C. Claussen, and E. Schöll, Partial synchronization in empirical brain networks as a model for unihemispheric sleep, Europhys. Lett. **126**, 50007 (2019).

[61] M. Gerster, R. Berner, J. Sawicki, A. Zakharova, A. Škoch, J. Hlinka, K. Lehnertz, and E. Schöll, FitzHugh-Nagumo oscillators on complex networks mimic epileptic-seizure-related synchronization phenomena, Chaos **30**, 123130 (2020).

[62] I. Omelchenko, A. Provata, J. Hizanidis, E. Scholl, and P. Hovel, Robustness of chimera states for coupled FitzHugh-Nagumo oscillators, Phys. Rev. E **91**, 022917 (2015).

[63] S. Huo, C. Tian, L. Kang, and Z. Liu, Chimera states of neuron networks with adaptive coupling, Nonlinear Dyn. **96**, 75 (2019).

[64] A. Rontogiannis and A. Provata, Chimera states in FitzHugh–Nagumo networks with reflecting connectivity, Eur. Phys. J. B **94**, 97 (2021).

[65] Y. Kuramoto, in *Chemical Oscillations, Waves, and Turbulence*, edited by H. Haken, Springer Series in Synergetics, Vol. 19 (Springer, Berlin, 1984).

[66] A. L. Hodgkin and A. F. Huxley, A quantitative description of membrane current and its application to conduction and excitation in nerve, J. Physiol. **117**, 500 (1952).